Hindawi
Wireless Communications and Mobile Computing
Volume 2022, Article ID 7228511, 13 pages
https://doi.org/10.1155/2022/7228511

Research Article

Abnormal Communication Signals Recognition Based on Image Enhancement and Improved Memory-Augmented Autoencoder

Tingyan Kuang,[1] Bo Zhou,[1] Jie Li,[1] Guoru Ding,[2] and Qihui Wu[1]

[1]*Key Laboratory of Dynamic Cognitive System of Electromagnetic Spectrum Space, Ministry of Industry and Information Technology, Nanjing University of Aeronautics and Astronautics, Nanjing 210016, China*
[2]*College of Communications Engineering, Army Engineering University, Nanjing 211106, China*

Correspondence should be addressed to Bo Zhou; b.zhou@nuaa.edu.cn

Received 14 June 2022; Revised 11 July 2022; Accepted 12 July 2022; Published 28 July 2022

Academic Editor: Mingqian Liu

Detecting increasing anomalous signals is critical to effective spectrum management due to the complexity of the use of electromagnetic spectrum. The anomaly recognition approach based on autoencoder (AE) heavily relies on the assumption that the reconstruction error of normal signals is generally lower than that of abnormal signals. Unfortunately, such an assumption does not necessarily hold due to the excessive generalization ability of the AE. The memory-augmented autoencoder model (MemAE) has been recently proposed to address this issue by introducing memory modules. Still, the standard MemAE model performs poorly on complex image datasets, and its performance for abnormal communication signals recognition is unknown. Therefore, we propose an image enhancement and improved memory-augmented autoencoder model (IIMemAE) to recognize abnormal communication signals. Specifically, we consider two key factors, i.e., the existence of redundant information in the time-frequency spectrogram and the low recognition accuracy of normal signals of the standard MemAE model. We introduce an image enhancement module and an anomaly determination module compared with the standard MemAE model. The proposed IIMemAE model can address the issue that the performance of anomaly recognition may be degraded due to the imbalanced communication signals in the real world. The simulation results show that IIMemAE can effectively recognize synthetic abnormal communication signals even at low signal-to-noise ratio (SNR) and jamming-to-signal ratio (JSR) conditions and outperform the standard MemAE model. Besides, the parametric Pauta criterion proposed can balance the recognition accuracy of normal and abnormal signals to meet the need for diverse recognition tasks.

1. Introduction

The electromagnetic spectrum is one of our most critical, widely used, and limited natural resources [1, 2]. With the advent of new wireless communication technologies, spectrum usage has become very complex, leading to radio wave congestion and other jamming issues [3]. Wireless spectrum anomalies may occur due to spectrum abuse or jamming. To effectively regulate the radio spectrum and improve the quality of service for wireless communications, it is crucial to analyze and detect anomalous behaviors in the electromagnetic spectrum.

Various communication antijamming technologies [4–6] and anomaly identification technologies [7, 8] have emerged to ensure the reliable transmission of information. In the wireless communication networks, the authors in [9] propose to detect interference by comparing the predicted packet delivery rate with the actual packet delivery rate. The authors in [10] focus on improving network performance under active jamming attacks to achieve jamming suppression. For spectrum anomaly identification, the characteristics of the communication signals can be exploited, as commonly done in the existing literature, such as [11–13]. The work in [11] proposes a cross-layer framework, which enables to detection of anomalous spectrum usage attacks (ASUA) in radio ad hoc networks by collecting the physical and network layer information. The authors in [12] propose a spectrum anomalous usage detection method using the

spatial distribution characteristics of the received signal strength. A typical spectrum is proposed based on feature extraction and a clustering algorithm to analyze spectral data in the broadcast bands [13].

However, these methods in [11–13] based on feature extraction could be of high computational complexity and consume lots of manpower and time [14]. In recent years, deep learning (DL) has achieved excellent performance in the radio field, such as interference identification [15] and spectrum anomaly detection [16]. A supervised learning-based scheme for signal detection and localization is proposed in [17], where a classification model is built by manually labeling each training sample. However, due to the complex electromagnetic spectrum situation and the unpredictable characteristics of anomalous signals, it is significantly difficult to collect and label a sufficient number of abnormal signals. Furthermore, communication signals in real-world systems are generally imbalanced. Abnormal communication signals can take many forms from the presence of unwanted signals in licensed bands to the absence of expected signals [18], which makes there are more abnormal signals than normal signals. Therefore, the performance of anomaly recognition methods based on supervised learning may be greatly degraded [19].

More recently, the unsupervised autoencoder (AE) learning model has emerged and has been adopted for anomaly detection with imbalanced data [20–25]. In network intrusion detection systems, the authors in [21] propose to employ a multimodal deep autoencoder (DAE) to detect abnormal traffic in the network and forward the anomaly to an attack classifier for classification. The authors in [22] use an ensemble of autoencoders to propose an online network traffic anomaly detection approach that can detect various attacks with performance comparable to offline anomaly detectors. In the anomaly recognition task, the AE is trained by minimizing the reconstruction error of normal signals, for which the reconstruction error is used as the anomaly metric. In [23], a deep autoencoder network is applied to detect the anomalies by reconstructing the spectrogram of the received signal. An unsupervised anomaly identification method based on the convolutional autoencoder (CAE) is studied in [24] to identify radio frequency interference. The authors in [25] propose a variational autoencoder- (VAE-) based spectral anomaly detection method for unlicensed bands, where the percentile (PER) score is introduced as a new measure of anomaly. Note that, the effectiveness of these AE models for anomaly recognition heavily relies on the assumption that the reconstruction error of normal signals is generally lower than that of abnormal signals.

However, this assumption does not necessarily hold as the abnormal signals may also be reconstructed well by the AE due to its strong generalization ability [26–28]. For example, if abnormal and normal signals share some common compositional features, a "strong" AE may also reconstruct the anomalies well. Thus, the reconstruction errors of the normal signals and some abnormal signals could be close to each other. Further, as there are generally no training samples of abnormal signals, it is impossible to predict the reconstruction results of abnormal signals. To address this issue, introduces a memory-augmented autoencoder (MemAE) to enlarge the reconstruction error of anomalous samples, thereby improving anomaly detection performance. However, the MemAE model does not achieve satisfactory performance for the anomaly recognition with complex image datasets (e.g., CIFAR-10), and its performance remains unknown for the datasets with abnormal communication signals. Moreover, the reconstruction error is used as the only criterion in [29] to determine whether a signal sample is normal or not. This, however, does not fully exploit the statistics (e.g., the mean and the variance) of the reconstruction error, which may be applied to define a more appropriate detection metric.

In this paper, we propose an unsupervised abnormal signal recognition algorithm based on image enhancement and improved memory-augmented autoencoder (IIMemAE). The main contributions can be described as follows:

(i) We consider an abnormal signal recognition model based on unsupervised learning. To the best of our knowledge, this work is the first attempt to apply the MemAE model in abnormal communication signals recognition

(ii) We propose an abnormal signal recognition algorithm based on image enhancement and improved memory-augmented autoencoder (IIMemAE). Specifically, we introduce an image enhancement module and an anomaly determination module to the standard MemAE model. Instead of using the reconstruction error directly, a parametric Pauta criterion is proposed to measure the anomaly of the reconstruction error of the signal

(iii) We evaluate the performance of various aspects of the IIMemAE model to verify its effectiveness and stability. The simulation results show that the average AUC (area under curve) value of the proposed method is greater than 80% even when the SNR is 2 dB and is close to 70% at the JSR is -5 dB. Compared to the standard MemAE model, the proposed IIMemAE model achieves better and more stable recognition performance, especially under low SNR and JSR conditions. Additionally, simulation results demonstrate that the anomaly determination module based on the parametric Pauta criterion proposed can balance the recognition accuracy of normal and abnormal signals and meet the need for different recognition tasks

The remainder of this paper is organized as follows. Section 2 introduces an abnormal signal recognition system model based on unsupervised learning. The function of each module of the IIMemAE model is presented in Section 3. Section 4 presents and analyzes the simulation results. Section 5 concludes the paper.

Notations: Matrices and vectors are in bold capital and bold lower cases, respectively. Number fields are in blackboard bold. The notations $|\bullet|$, $\|\bullet\|_1$, and $\|\bullet\|_2$ represent absolute value, ℓ_1-norm, and ℓ_2-norm, respectively.

2. System Model

As shown in Figure 1, we consider an abnormal signal recognition model in a wireless communication system. In addition to legitimate signals, there may be malicious or illegal signals in the signals received by the receiver in this system model. Then, the anomaly recognition module on the receiver accomplishes the reconstruction and anomaly recognition of the signal received.

We consider two ways to define abnormal signals. One is for unauthorized signals, that is, signals sent from illegal transmitters without the authorization of radio regulatory agencies. The other is an authorized signal, which suffered external malicious jamming or failures that occur on the receiver during transmission. In specific, for nonstationary signals, abnormal signals can be described as the following:

(i) The signal is legal, but the parameters such as the bandwidth and the center frequency of the signal are not within the specified range

(ii) This is one synthetic anomaly, where legal signals coexist with jamming signals and the jamming signal parameters are legal

The primary task of abnormal communication signals recognition is to identify whether the received signal is normal or abnormal. In this paper, we focus on the second type of anomaly (the abnormal signal recognition for the first type is left to future work.), and the abnormal signal is modeled as follows:

$$S_1(t) = S_0(t) + S_j(t), \tag{1}$$

where $S_0(t)$ denotes the normal signal received and $S_j(t)$ denotes the jamming.

The jamming-to-signal ratio (JSR) can be expressed as follows [30]:

$$\mathrm{JSR} = 10 \log_{10} \frac{P_j}{P_s}, \tag{2}$$

where P_j and P_s denote the jamming power and the signal power, respectively.

The problem of abnormal signal recognition can be formulated as a binary hypothesis test:

$$\begin{aligned} H_0 &: r(t) = S_0(t)C_0(t) + n(t), \\ H_1 &: r(t) = S_1(t)C_1(t) + n(t), \end{aligned} \tag{3}$$

where $r(t)$ denotes the received signal, $C_0(t)$ and $C_1(t)$ represent the channel of the normal signal and the channel of the abnormal signal, respectively, and $n(t)$ is the additive Gaussian white noise with zero mean and variance σ^2. The null hypothesis H_0 represents the absence of abnormal signals in the communication system operation, and the alternative hypothesis H_1 represents the presence of abnormal signals.

The variation of a signal in the time and frequency domains is the most crucial feature in spectrum usage. Time-frequency analysis can extract the characteristic information of communication signals at a specific time and frequency, accurately reflecting the relationship between the signal frequency and the time change. Therefore, the smooth pseudo Wigner-Ville distribution (SPWVD) [31] is performed to obtain a two-dimensional time-frequency spectrogram of the received signal as follows:

$$W_x(t,f) = \int g(u-t) \int h(\tau) s\left(t + \frac{\tau}{2}\right) s * \left(t - \frac{\tau}{2}\right) e^{-j2\pi f t} d\tau du, \tag{4}$$

where $g(u-t)$ and $h(\tau)$ are real symmetric window functions and s^* denotes the conjugate of s. In particular, $g(u-t)$ allows cross-terms oscillating parallel to the time axis to perform smoothing (i.e., time smoothing), and $h(\tau)$ allows smoothing of cross-terms oscillating parallel to the frequency axis (i.e., frequency smoothing). Since smoothing is performed in both the time and frequency domains, the cross-interference terms of multicomponent signals can be well suppressed.

3. IIMemAE-Based Abnormal Signal Recognition Algorithm

In this section, we introduce the structure of IIMemAE and its implementation in abnormal signal recognition.

3.1. Overview. As shown in Figure 2, the proposed IIMemAE model consists of five main components: an image enhancement module, an encoder, a decoder, a memory enhancement module, and an anomaly determination module. In specific, the image enhancement module first improves the contrast of the time-frequency spectrogram of the signal. The encoder encodes the time-frequency spectrogram of the signal and generates query terms. The memory enhancement module includes addressing operations for recording normal signal patterns and retrieving the memory items, which are then passed to the decoder for reconstruction. The IIMemAE model does not decode directly through the decoder like standard autoencoders. Instead, the encoded results are used as query terms to retrieve normal signal patterns in memory enhancement modules and update memory terms through attention-based addressing operations.

Finally, the query result is inputted into the decoder for reconstruction. In the training process, the IIMemAE model proposed is trained by minimizing the reconstruction error and the entropy loss of the query weight of memory items. In the test phase, the model performs reconstruction using only a limited number of normal signal patterns recorded in memory. The anomaly determination module quantifies the abnormality degree of the signal according to a parametric Pauta criterion.

3.2. Image Enhancement Algorithm. The time-frequency grayscale image converted from a communication signal has low contrast, and low-contrast images result from a lack

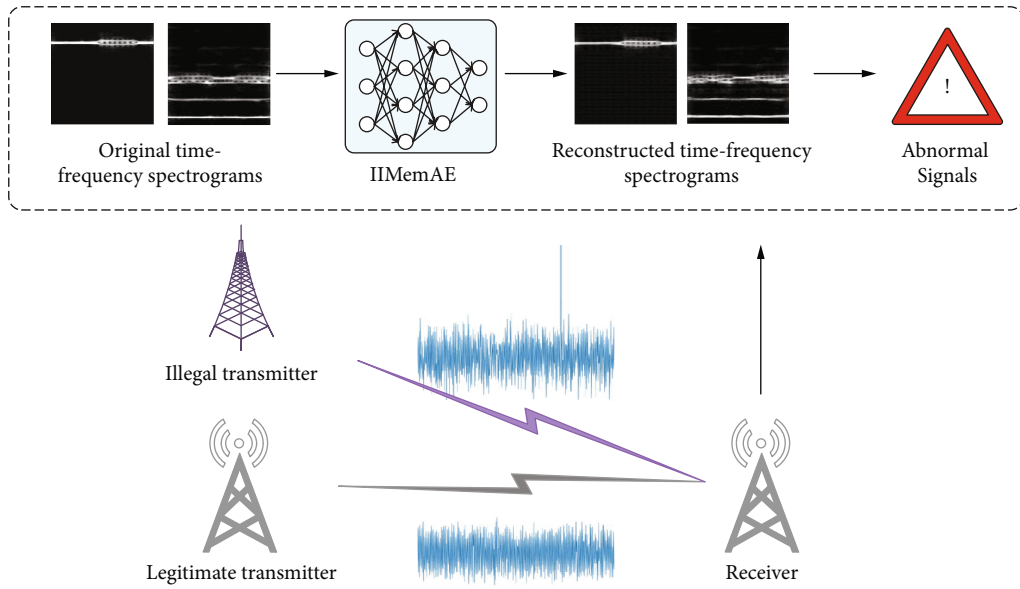

Figure 1: Abnormal signal recognition model structure.

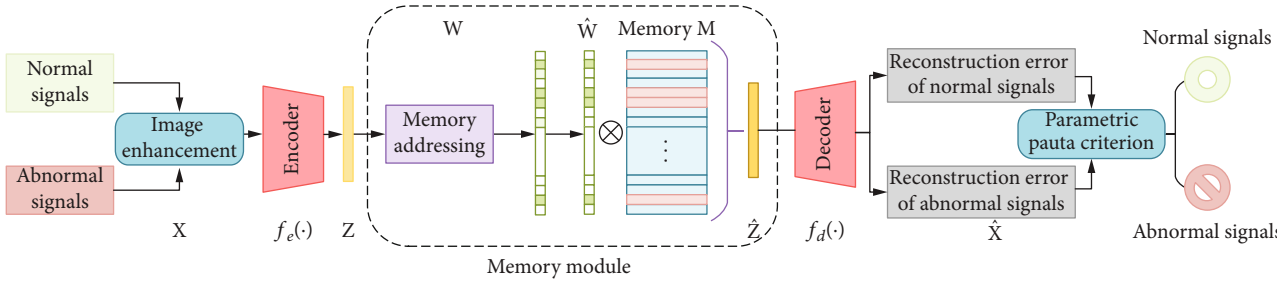

Figure 2: Diagram of the proposed IIMemAE.

of dynamic range in the imaging pixels, which may induce the model to extract incorrect features and false matches [32]. By contrast stretching, the effect of redundant pixels in image features is reduced. Hence, we introduce an image enhancement module and apply the classical image grayscale transformation to the time-frequency grayscale image. The basic principle of the image grayscale transformation is to map the gray value of the original grayscale image to a specified range of grayscale values of the output image. By saturating parts of the time-frequency grayscale image at the lowest and highest grayscales, the contrast of the output image can be improved. In this paper, the grayscale transformation of a time-frequency spectrogram can be expressed as follows:

$$\hat{o} = r\left(o, [p_1\, p_2], [q_1\, q_2]\right), \quad p_1 < p_2, q_1 < q_2, \tag{5}$$

where o denotes the original image, $\hat{o}$ denotes the image after grayscale transformation, and $r(\bullet)$ denotes the grayscale transformation function. The values of points (p_1, q_1) and (p_2, q_2) control the shape of the transformation function. In transforming the grayscale of the original image o to the new image $\hat{o}$, the grayscale value of the pixels in o whose grayscale value is lower than p_1 is assigned as q_1 in $\hat{o}$. Similarly, the gray value of the pixel in f whose gray value is higher than p_2 is also assigned as q_2 when it is transformed to $\hat{o}$.

For the gray value p of any pixel in the original image, the gray value $\hat{p}$ of the corresponding pixel in the new image is obtained after transformation. For example, the transformation processing can be given as follows:

$$\hat{p} = \begin{cases} 255p_1, & p < p_1, \\ \dfrac{q_2 - ql}{p_2 - p_1} \times (p - p_1) \times 255 + 255q_1, & p_1 < p < p_2, \\ 255p_2, & p < p_2. \end{cases} \tag{6}$$

3.3. Encoder and Decoder. The encoder and the decoder generally have a symmetrical structure. The input time-frequency spectrogram dataset sample space is represented as $\mathbb{X}$. When an input $\mathbf{x} \in \mathbb{X}$ is given, the encoder converts it into an encoded $\mathbf{z} \in \mathbb{Z}$ in the low-dimensional feature space. The decoder is trained to reverse map a latent

representation $\hat{\mathbf{z}} \in \mathbb{Z}$ to the domain $\mathbb{X}$. The above process can be expressed as follows:

$$\mathbf{z} = f_e(x; \theta_e), \tag{7}$$

$$\hat{x} = f_d(\hat{\mathbf{z}}; \theta_d), \tag{8}$$

where θ_e and θ_d denote the parameters of the encoder and the decoder, respectively. Here, $\mathbf{z}$ is used as a query to retrieve the relevant items in memory. Then, these items $\mathbf{z}$ are collected and fed to the decoder. Note that, for the standard AE model, $\mathbf{z}$ is set to be $\mathbf{z}$ [33].

3.4. Memory Enhancement Module. The memory enhancement module is designed as a matrix $\mathbf{M} \in \mathbb{R}^{N \times C}$, including N real-valued vectors of dimensions C. The dimension C of each memory item is the same as the dimension of the encoder encoding result $\mathbf{z}$. The hyperparameter N defines the maximum capacity of memory.

$$\hat{\mathbf{z}} = \mathbf{w}\mathbf{M} = \sum_{i=1}^{N} w_i m_i, \tag{9}$$

where $\mathbf{z}$ is obtained by soft addressing of weight vector $\mathbf{w} \in \mathbb{R}^{1 \times N}$ and memory $\mathbf{M}$. $\mathbf{w} = [w_i]_{i=1,2,\cdots,N}$ is a row vector with nonnegative entries that sum to one. The memory $\mathbf{M}$ records the various prototypical normal patterns during training. The weight vector $\mathbf{w}$ is obtained from $\mathbf{z}$ and calculated by the softmax operation in Equation (10), where d is the similarity measure, defined as cosine similarity.

$$w_i = \frac{\exp\left(d(\mathbf{z}, m_i)\right)}{\sum_{j=1}^{N} \exp\left(d\left(\mathbf{z}, m_j\right)\right)}. \tag{10}$$

In addition, the memory module can increase sparsity by hard shrinking the weight vector $\mathbf{w}$ in Equation (11). Sparse addressing encourages fewer but more relevant memory items to represent query results, improving the representation accuracy of memory items.

$$\hat{w}_i = h(w_i; \lambda) = \begin{cases} w_i, & \text{if } w_i > \lambda, \\ 0, & \text{otherwise}, \end{cases} \tag{11}$$

where λ denotes the shrinkage threshold and $\hat{\mathbf{w}}$ denotes the sparse weight vector. The elements in the weight vector $\mathbf{w}$ that are less than or equal to the threshold value are assigned as 0 to realize the sparsity of the vectors. However, it is not easy to calculate the backpropagation of discontinuous functions. To simplify the calculation, we employ the continuous ReLU function to realize the shrinking operation as follows:

$$\hat{w}_i = \frac{\max\left(w_i - \lambda, 0\right) \bullet w_i}{|w_i - \lambda| + \varphi}, \tag{12}$$

where φ is a very small constant. The standardized operation shall be carried out again when the shrinkage is completed as follows:

$$\hat{w}_i = . \tag{13}$$

3.5. Anomaly Determination Module. By querying the memory module, all prototype vectors are considered instead of the nearest prototype vectors, which solves the problem of the excessive generalization ability of the AE. This means that the reconstruction error for abnormal samples is enlarged, making recognition easier. The next phase is to design an appropriate threshold to separate the two classes instead of directly using the average reconstruction error as a metric. In the testing phase, the decoder outputs the reconstruction loss L_r for all test samples and compares it with a predefined threshold η, which can be expressed as follows:

$$L_r \underset{H_o}{\overset{H_1}{\gtrless}} \eta. \tag{14}$$

To design an appropriate threshold, the Pauta criterion [34] is introduced:

$$A_n = |e_n - \bar{e}| > 3\sigma, \tag{15}$$

where e_n denotes the reconstruction error and $\bar{e}$ and σ denote the mean and standard deviation of the reconstruction error of the normal signal. To make the Pauta criterion more accommodation for the abnormal signal recognition task, we modified the Pauta criterion as follows:

$$A_n > K\sigma, \tag{16}$$

where K denotes a positive constant. If the reconstruction error of the time-frequency spectrogram of the input signal satisfies the above formula, the signal is recognized as an abnormal signal. Otherwise, the signal is recognized as a normal signal.

3.6. Training. The training loss comprehensively considers the reconstruction loss and the entropy loss. Given a training dataset $D = \sum_{i=1}^{T} x_i$ containing T time-frequency spectrograms of normal signals, let $\hat{x}_i$ be the reconstruction time-frequency spectrogram corresponding the each training time-frequency spectrogram x_i. The minimized reconstruction error for each time-frequency spectrogram can be expressed as follows:

$$L_r(x_i, \hat{x}_i) = \|x_i, \hat{x}_i\|_2^2, \tag{17}$$

where the reconstruction error is replaced by ℓ_2-norm. The entropy loss improves the sparsity of the generated address weights during training. We minimize the entropy loss:

$$L_e(\hat{w}_i) = -\sum_{i=1}^{T} \hat{w}_i \log\left(\hat{w}_i\right). \tag{18}$$

Combining Equations (17) and (18), the training loss of IIMemAE is described as follows:

$$L = \frac{1}{T}\sum_{i=1}^{T}(L_r(x_i, \hat{x}_i) + \alpha L_e(\hat{w}_i)), \tag{19}$$

where α denotes a hyperparameter. The memory $\mathbf{M}$ is updated by backpropagation and gradient descent during training.

Specifically, there are three primary stages for the implementation of the abnormal communication signals recognition system:

(1) Signal reception: In the communication system operating, the receiver performs time-frequency processing on all received signals to obtain time-frequency spectrograms. The time-frequency spectrograms are then processed with an image enhancement algorithm

(2) Training IIMemAE: Since the normal communication signal is known to the system, the IIMemAE model can be pretrained by the time-frequency spectrogram of the normal communication signal, which is considered to memorize the characteristics of the normal communication signal. The time-frequency spectrogram used in training should also be processed via the image enhancement algorithm

(3) Anomaly recognition: All the time-frequency spectrograms obtained in (1) are used as the input of the IIMemAE model, which reconstructs all the time-frequency spectrograms. The parametric Pautu criterion measures the threshold. If the reconstruction error is larger than the threshold, it is considered an abnormal signal. Otherwise, it is considered to be a normal signal

4. Simulation Results and Discussion

In this section, the performance of the proposed IIMemAE model and its variants are evaluated through extensive simulations. The standard MemAE [29] serves as the baseline under identical conditions. All models are trained with the Adam optimizer of a learning rate of 0.01 for a maximum of 100 epochs. The hyperparameter α is 0.0002. All models are implemented based on the Pytorch framework and trained by using an NVIDIA GTX1080 GPU.

4.1. Simulation Setup. In this paper, the BPSK signal as the normal signal is obtained by simulation. Any remaining signal that is not a BPSK signal is considered anomalous, and we simulate six typical synthetic anomalies [35, 36]. (i) *Comb-spectrum*: the comb spectrum jamming consists of multiple identically modulated subjammings. It is a set of narrowband interferers modulated over a range of frequencies. Each subjamming is superimposed in the time domain and separated in the frequency domain. The jamming spectrum is comb-shaped. (ii) *Multitone*: the multitone jamming consists of multiple tones. Each frequency point is randomly distributed in a specific frequency band. (iii) *Pulse*: the pulse jamming transmitted at a random time on a fixed frequency band. (iv) *Single-tone*: single-tone jamming can affect the BPSK signal by generating high power. (v) *Sweeping*: it performs linear frequency sweep jamming on the BPSK signal, and the center frequency of the jamming is the same as the BPSK signal. (vi) *Noise-FM*: the noise FM jamming with a certain bandwidth and high power is added to the BPSK signal.

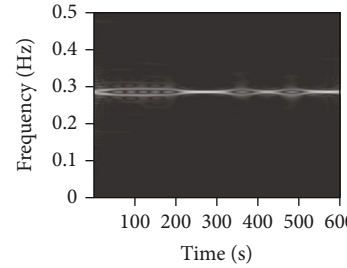

Figure 3: Time-frequency spectrograms of one normal signal.

The time-frequency spectrograms of one normal signal are shown in Figure 3 and six abnormal signals are shown in Figure 4. The training dataset contains 2000 normal time-frequency spectrograms, each of size 112×112. The testing dataset contains 1400 time-frequency spectrograms with 200 normal time-frequency spectrograms and 1200 anomalous time-frequency spectrograms. Each abnormal signal mentioned above has 200 time-frequency spectrograms, each of which is of size 112×112. The training and testing datasets are not duplicated. The test dataset's 200 time-frequency spectrograms of the normal signal are taken out as the validation dataset.

The implementation of the IIMemAE model to recognize abnormal signals can be described as follows:

(1) The training dataset and test dataset are processed by the image enhancement algorithm. Then, the training dataset is fed into the network to train. Only the time-frequency spectrogram of normal signals is trained during training. Figure 5 shows an example of the samples processed by the image enhancement algorithm

(2) Input the validation dataset into the trained network to obtain the reconstruction error of the normal signal timefrequency spectrogram. The threshold η is measured by the mean and variance of the reconstruction error

(3) Input the test dataset into the trained network and get the reconstruction error of each time-frequency spectrogram. Comparing the reconstruction error with the threshold η, if the reconstruction error of a time-frequency spectrogram satisfies the parametric Pauta criterion in Equation (16), it is considered an abnormal signal. On the contrary, it is considered a normal signal

As commonly done in the literature [20, 29], we use the AUC value as the evaluation index of all models, which is the area under the ROC (receiver operation characteristic)

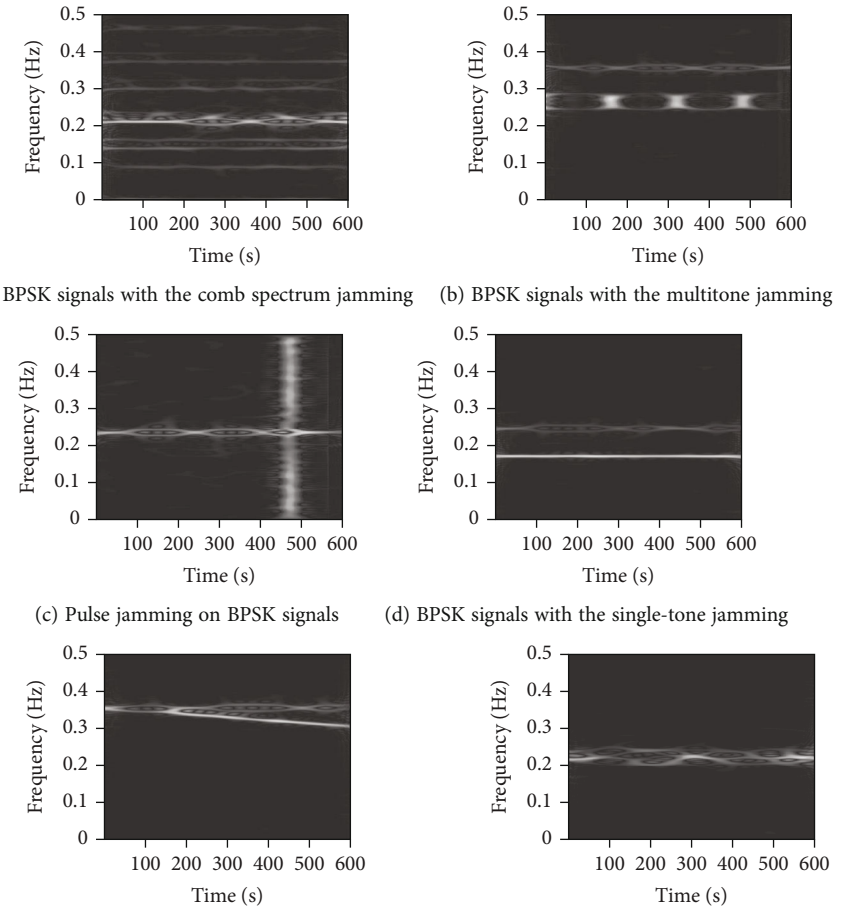

(a) BPSK signals with the comb spectrum jamming (b) BPSK signals with the multitone jamming

(c) Pulse jamming on BPSK signals (d) BPSK signals with the single-tone jamming

(e) Linear frequency sweeping jamming on BPSK signals (f) BPSK signals with the noise FM jamming

Figure 4: Time-frequency spectrograms of six abnormal signals.

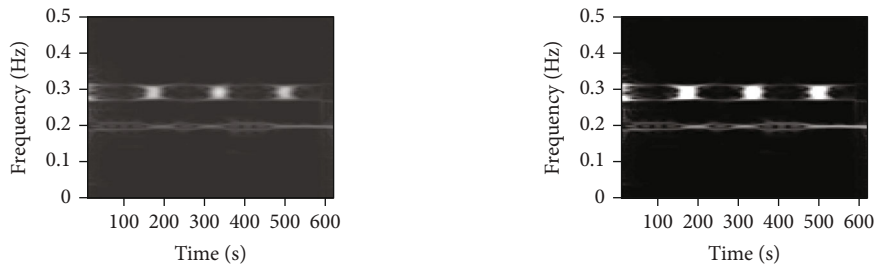

(a) The original time-frequency spectrogram (b) The time-frequency spectrogram after image enhancement processing

Figure 5: The time-frequency spectrogram of the *multitone* abnormal signal before and after image enhancement algorithm processing.

Table 1: Experimental results of different models.

Model	TP	TN	$F1$-score	AUC
MemAE	67.26	99.45	78.86	83.36
MemAE (IE)	59.83	99.47	73.36	79.65
MemAE ($K = 3$)	98.40	83.03	65.79	90.71
IIMemAE ($K = 3$)	**98.88**	92.10	80.31	**95.49**
IIMemAE ($K = 0.3$)	69.10	**99.54**	**80.40**	84.32

curve. We also consider the $F1$-score, which represents the harmonized average of precision and recall. It is a metric primarily used to assess imbalanced data accurately [37]. Table 1 shows the average AUC values for 20 tests on the signal dataset. The memory capacity N is 1000, the signal-to-noise ratio (SNR) is 10 dB, and the JSR is 5 dB.

As shown in Table 1, the proposed IIMemAE outperforms the standard MemAE. In particular, all evaluation metrics of IIMemAE at $K = 0.3$ outperform the standard MemAE.

Table 2: The computational complexity of the presented IIMemAE model, IIMemAE's variants, and the standard MemAE model.

	IIMemAE ($K = 0.3$)	IIMemAE ($K = 3$)	MemAE ($K = 3$)	MemAE (IE)	MemAE
Running time (s)	0.01599	0.01627	0.01524	0.01613	0.01495

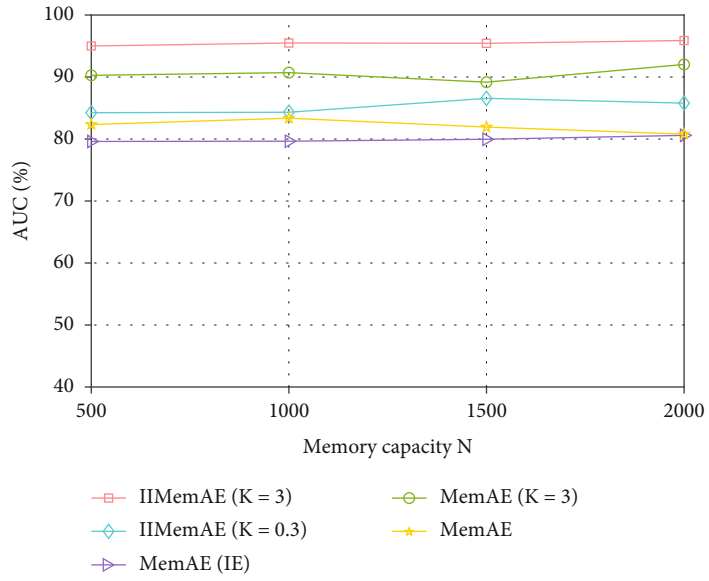

Figure 6: Robustness to the setting of memory capacity. The AUC values of IIMemAE and its variants for different memory capacities on the abnormal.

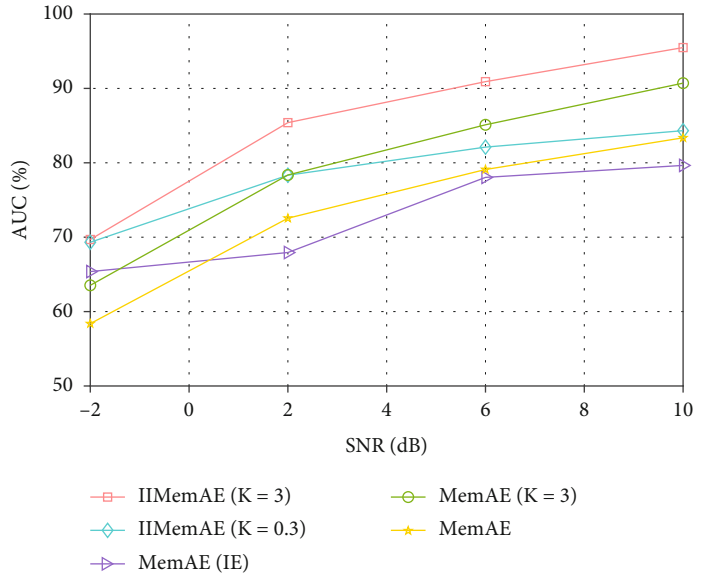

Figure 7: AUC of different SNRs for each model with the JSR of 5 dB.

Specifically, the model with anomaly determination module significantly outperforms MemAE without parametric Pauta criterion and exhibits higher TP (true positive). From the mean TN (true negative), MemAE (IE) can produce better results than the standard MemAE. We can conclude from Table 1 that the image enhancement module can improve the recognition accuracy of abnormal signals, and the abnormal judgment module can improve the recognition accuracy of normal signals. The IIMemAE proposed in this paper comprehensively considers the effect of the two modules on the overall recognition accuracy. Therefore, IIMemAE can yield better performance than the standard MemAE.

Moreover, we empirically study the computational complexity of the proposed method on the test dataset (i.e., contains 1400 time-frequency spectrograms) using NVIDIA GTX1080 GPU. As shown in Table 2, the proposed

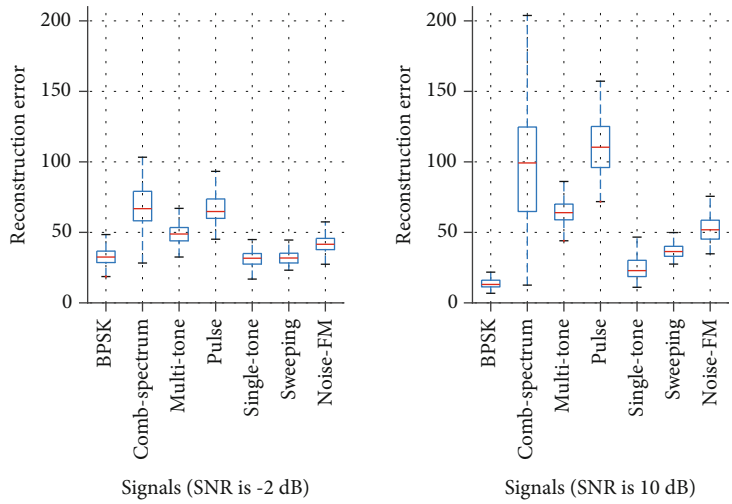

FIGURE 8: Boxplots of reconstruction error for each signal by the IIMemAE ($K = 3$) model. On the left is the reconstruction error distribution with an SNR of -2 dB. On the right is the reconstruction error distribution with an SNR of 10 dB.

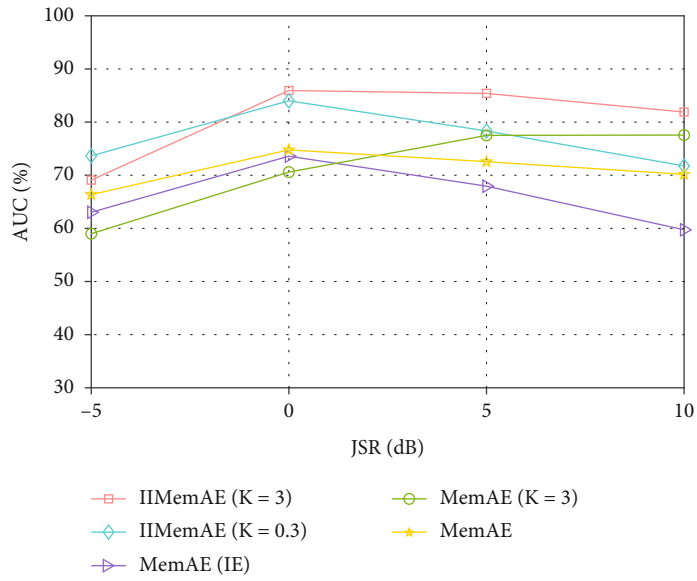

FIGURE 9: AUC of different JSRs for each model with the SNR of 2 dB.

IIMemAE ($K = 3$) averagely takes 0.01627 seconds to recognize a time-frequency spectrogram. Compared to the standard MemAE model that takes 0.01495 seconds for each time-frequency spectrogram, our image enhancement module and anomaly determination module induce little additional computational time (i.e., 1.32×10^{-3} seconds per time-frequency spectrogram).

4.2. Impact of Different Memory Capacities. We conduct experiments by setting different memory capacities, and the AUC values are shown in Figure 6. For the anomalous signal datasets, the AUC of the model is always stable even as the dimension of the memory matrix increases. It indicates that IIMemAE is insensitive to memory capacity N and can robustly produce credible results. In addition, simulation results of other models show that they are equally stable and robust. All models have AUC values of 80% and above, with IIMemAE ($K = 3$) performing the best. Compared with the standard MemAE, IIMemAE and MemAE ($K = 3$) can produce better AUC values. The MemAE (IE) does not perform well as the standard MemAE because it has worse TP values.

4.3. Impact of Different SNRs. As shown in Figure 7, with the increase of SNR, the AUC values of the five models increase. Overall, MemAE (IE) shows the worst performance, and IIMemAE ($K = 3$) offers the best performance. However, it is worth noting that the standard MemAE performs the worst at low SNR. These models with the image enhancement module and anomaly determination module can produce good recognition results even at low SNR.

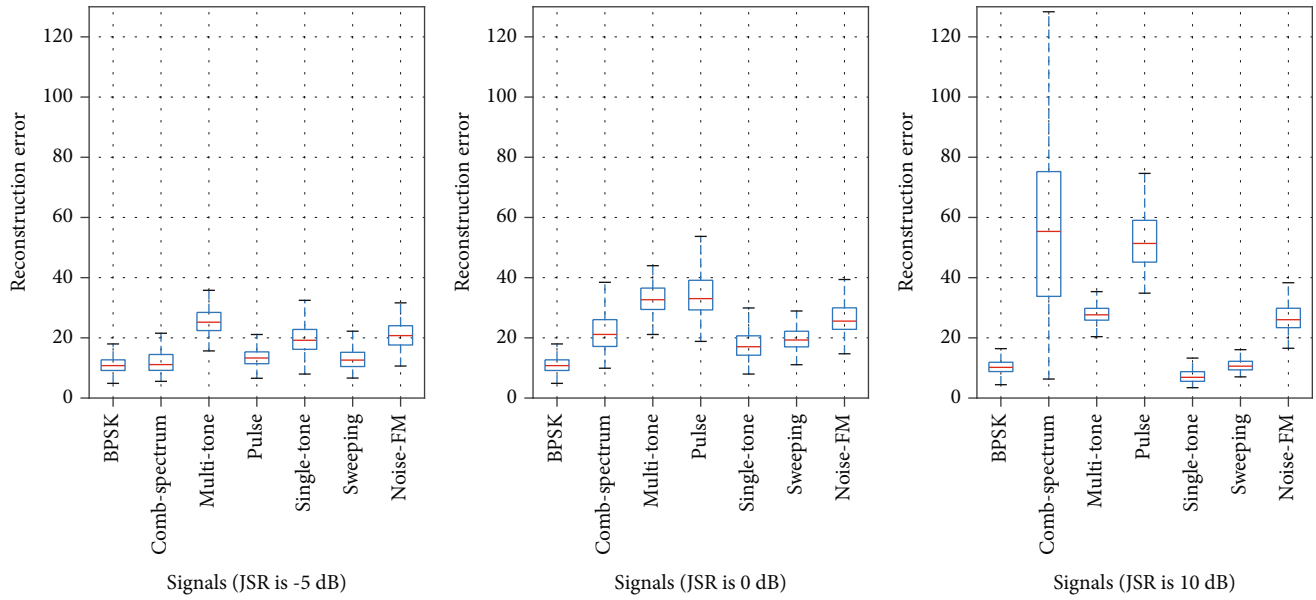

FIGURE 10: Boxplots of reconstruction error for each signal by the IIMemAE ($K = 3$) model. On the left is the reconstruction error distribution with a JSR of -5 dB. In the middle is the reconstruction error distribution with a JSR of 0 dB. On the right is the reconstruction error distribution with a JSR of 10 dB.

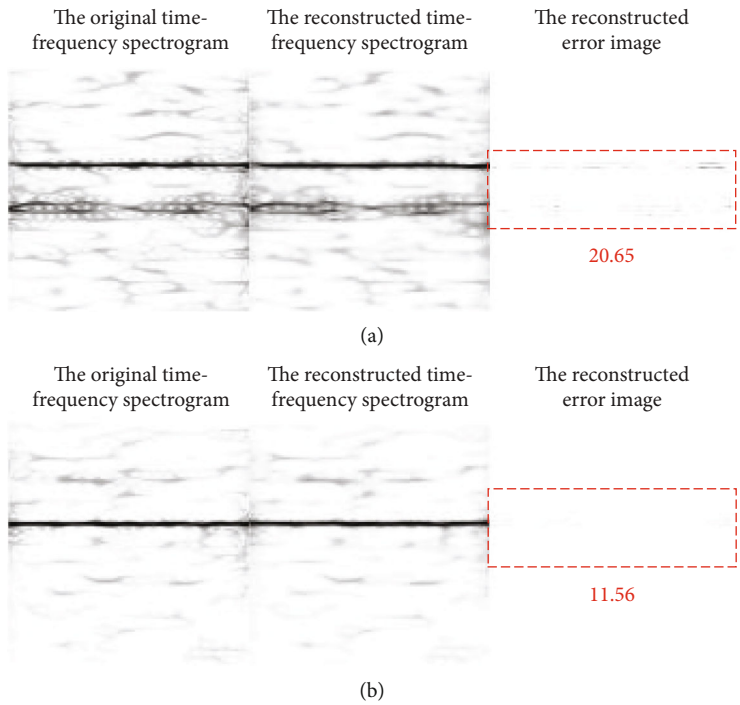

FIGURE 11: The reconstruction results of the abnormal signal single-tone by IIMemAE ($K = 3$). (a) The reconstruction results of IIMemAE ($K = 3$) with a JSR of 0 dB. (b) The reconstruction results of IIMemAE ($K = 3$) with a JSR of 10 dB.

Figure 8 shows the reconstruction error distribution for each signal under the IIMemAE ($K = 3$) model. In the boxplots, the upper and lower bounds of the box in blue are the upper and lower quartiles of one signal reconstruction error, respectively. Therefore, the width of the box reflects the degree of fluctuation in the reconstruction error of each signal. The red line segment in the middle of the box represents the median of each signal reconstruction error. SNR is -2 dB in the left boxplots, the average reconstruction error of the BPSK signal is 32.69, and the average reconstruction error of each abnormal signal is 71.69, 49.32, 66.80, 31.35, 32.75, and 42.88, respectively. SNR is 10 dB in the right boxplots, the average reconstruction error of the BPSK signal is 13.63, and the average reconstruction error of each

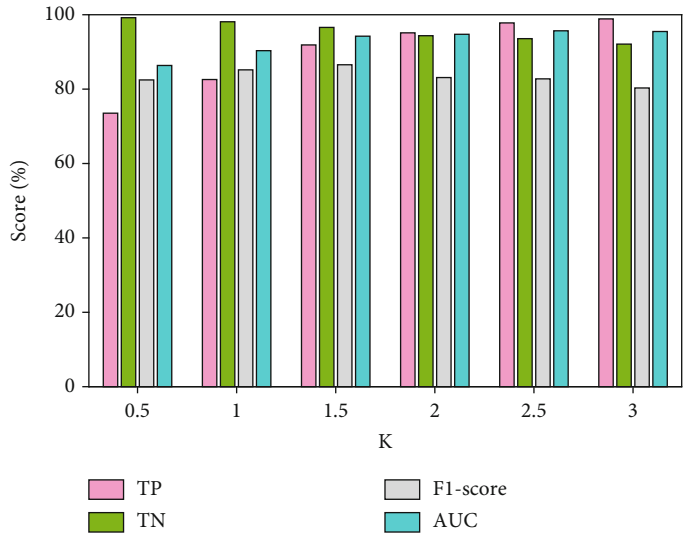

Figure 12: The influence of different parameters K in the IIMemAE model on the recognition performance of abnormal signals.

abnormal signal is 98.57, 64.27, 110.48, 26.09, 38.34, and 56.48, individually. As the SNR increases, the average reconstruction error of the BPSK signal decreases, while the average reconstruction error of the abnormal signal increases. Therefore, the larger the SNR, the IIMemAE model can better reconstruct normal signals and enlarge the reconstruction error of abnormal signals.

4.4. Impact of Different JSRs. Figure 9 shows the experimental results of setting different JSRs. Compared with the standard MemAE model, the IIMemAE ($K = 3$) model offers the best performance evaluated based on AUC. In particular, all models except MemAE ($K = 3$) perform best when JSR is 0 dB. Specifically, Figure 10 shows the reconstruction error distribution of each signal through the IIMemAE ($K = 3$) model at different JSRs. JSR is -5 dB in the left boxplots, the average reconstruction error of the BPSK signal is 11.06, and the average reconstruction error of each abnormal signal is 17.76, 25.75, 13.62, 19.86, 16.46, and 25.54, respectively. JSR is 0 dB in the middle boxplots, the average reconstruction error of the BPSK signal is 11.06, and the average reconstruction error of each abnormal signal is 26.74, 32.87, 34.71, 17.93, 22.15, and 28.71, individually. Since the parameter JSR is set based on the abnormal signal, it does not affect the reconstruction of the BPSK signal for the IIMemAE model. As the JSR increases, the IIMemAE model enlarges the reconstruction error of anomalous signals and thus can result in better performance.

However, when the JSR increases to a certain level, the performance of the IIMemAE model begins to decline. In Figure 10, JSR is 10 dB in the right boxplots, the average reconstruction error of each abnormal signal is 55.27, 27.97, 53.07, 7.47, 11.14, and 27.61, respectively. Compared with the middle boxplots at JSR of 0 dB, the reconstruction errors of abnormal signal *comb-spectrum* and *pulse* are enlarged. However, the reconstruction errors of abnormal signals *multitone*, *single-tone*, *sweeping*, and *noise-FM* are reduced instead. Particularly, the reconstruction errors of abnormal signal *single-tone* and *sweeping* are almost as same as the normal BPSK signal.

To see it more clearly, we further plot images for the experimental results, which are performed color reversion process in Figure 11. It shows the time-frequency spectrogram, the reconstructed time-frequency spectrogram, and the reconstructed error image of the abnormal signals *single-tone* with a JSR of 10 dB. Comparing the reconstructed error images at the JSR is 0 dB and 10 dB, the IIMemAE model can reconstruct the abnormal signal *single-tone* and *sweeping* well with the JSR of 10 dB. In Figure 11(a) and Figure 11(b), the reconstruction error is 20.65 and 11.56, respectively. Single-tone jamming and frequency sweeping jamming characteristics are similar to the BPSK signal characteristic. From the time-frequency spectrogram, they both look like a line segment. Therefore, the performance of the IIMemAE model begins to degrade at the JSR of 5 dB.

The synthetic abnormal signal in this paper is formed by the superimposition of the jamming signal on the normal recognition. Simulation results show that the IIMemAE model outperforms the standard MemAE model even at low SNR and JSR. Specifically, in the IIMemAE model, the image enhancement module can improve the recognition accuracy of abnormal signals, and the anomaly determination module can improve the recognition accuracy of normal signals. Moreover, the anomaly determination module with the parametric Pauta criterion can balance the recognition accuracy of normal and abnormal signals and adapt to diverse abnormal signal recognition tasks. Future works will investigate the image enhancement model to further improve the performance of the IIMemAE model for signals with similar features. Besides, more research work is needed to detect anomalies in real-time signal. When the JSR increases to a certain level, the time-frequency spectrogram of the synthetic abnormal signal will mainly display the characteristics of the jamming signal. If the characteristics

of the jamming signal are similar to the normal signal, the IIMemAE model will reconstruct the synthetic abnormal signal well, leading to its performance degradation. This issue also exists in the standard MemAE model and two variant models. We hope to address this issue in future work further.

4.5. Impact of Different K. Figure 12 shows the effect of different parameters K in the IIMemAE model on the recognition performance of abnormal signals with the SNR is 10 dB and the JSR is 5 dB. The evaluation indexes TP and AUC increase with the increase of K, and the $F1$-score fluctuates relatively stably within a certain range. However, the evaluation index TN decreases as K increases. It dictates that the size of K can balance the classification accuracy of positive samples and negative samples. In particular, TP and TN are above 94% when the parameter K is set to 2. Therefore, we can select an appropriate K value for the IIMemAE model to adapt to different abnormal signal recognition task requirements.

5. Conclusion

In this paper, we have proposed an IIMemAE model to improve the performance of abnormal communication signals recognition based on the MemAE model. The proposed IIMemAE model can address the issue that the performance of anomaly recognition may be degraded due to the imbalanced communication signals in the real world. We have considered two important issues, i.e., redundant information exists in the time-frequency spectrogram, and the recognition accuracy of normal signals based on the standard MemAE model is low. We have introduced an image enhancement module and an anomaly determination module. In particular, the image enhancement module can reduce the influence of redundant information in the time-frequency spectrogram, and the anomaly determination module based on the parametric Pauta criterion can be flexibly adjusted according to the need for anomaly or classify the detected anomalies.

Data Availability

The data that support the findings of this study are available from the corresponding author upon reasonable request.

Conflicts of Interest

The authors declare that they have no conflicts of interest.

Acknowledgments

This work is supported by the National Key R&D Program of China (No. 2018YFB1800800) and the National Natural Science Foundation of China (No. U20B2038, No. 61901520, No. 61931011, No. 61871398, No. 61827801, and No. 62101254).

References

[1] Q. Wu, G. Ding, J. Wang, and Y.-D. Yao, "Spatial-temporal opportunity detection for spectrum-heterogeneous cognitive radio networks: two-dimensional sensing," *IEEE Transactions on Wireless Communications*, vol. 12, no. 2, pp. 516–526, 2013.

[2] G. Ding, J. Wang, Q. Wu, Y.-D. Yao, F. Song, and T. A. Tsiftsis, "Cellular-base-station-assisted device-to-device communications in TV white space," *IEEE Journal on Selected Areas in Communications*, vol. 34, no. 1, pp. 107–121, 2016.

[3] S. Rajendran, V. Lenders, W. Meert, and S. Pollin, "Crowdsourced wireless spectrum anomaly detection," *IEEE Transactions on Cognitive Communications and Networking*, vol. 6, no. 2, pp. 694–703, 2020.

[4] M. Liu, B. Li, Y. Chen et al., "Location parameter estimation of moving aerial target in space–air–ground-integrated networks-based IoV," *IEEE Internet of Things Journal*, vol. 9, no. 8, pp. 5696–5707, 2022.

[5] H. Pirayesh and H. Zeng, "Jamming attacks and anti-jamming strategies in wireless networks: a comprehensive survey," *IEEE Communications Surveys Tutorials*, vol. 24, no. 2, pp. 767–809, 2022.

[6] M. Liu, C. Liu, M. Li, Y. Chen, S. Zheng, and N. Zhao, "Intelligent passive detection of aerial target in space-air-ground integrated networks," *China Communications*, vol. 19, no. 1, pp. 52–63, 2022.

[7] M. Liu, J. Wang, N. Zhao, Y. Chen, H. Song, and R. Yu, "Radio frequency fingerprint collaborative intelligent identification using incremental learning," *IEEE Transactions on Network Science and Engineering*, p. 1, 2021.

[8] A. Moumena, "Abnormal behavior detection of jamming signal in the spectrum using a combination of compressive sampling and intelligent bivariate k-means clustering technique in wideband cognitive radio systems," in *2015 4th International Conference on Electrical Engineering (ICEE)*, pp. 1–4, Boumerdes, Algeria, 2015.

[9] M. Spuhler, D. Giustiniano, V. Lenders, M. Wilhelm, and J. B. Schmitt, "Detection of reactive jamming in DSSS-based wireless communications," *IEEE Transactions on Wireless Communications*, vol. 13, no. 3, pp. 1593–1603, 2014.

[10] D. Ciuonzo, A. Aubry, and V. Carotenuto, "Rician mimo channel- and jamming-aware decision fusion," *IEEE Transactions on Signal Processing*, vol. 65, no. 15, pp. 3866–3880, 2017.

[11] C. Sorrells, P. Potier, L. Qian, and X. Li, "Anomalous spectrum usage attack detection in cognitive radio wireless networks," in *2011 IEEE International Conference on Technologies for Homeland Security (HST)*, pp. 384–389, Waltham, MA, USA, 2011.

[12] S. Liu, L. J. Greenstein, W. Trappe, and Y. Chen, "Detecting anomalous spectrum usage in dynamic spectrum access networks," *Ad Hoc Networks*, vol. 10, no. 5, pp. 831–844, 2012.

[13] H. Yan, B. Zhou, J. Liu, M. Kong, and Z. Pei, "Radio signal recognition based on constructing typical spectrum," in *2016 2nd IEEE International Conference on Computer and Communications (ICCC)*, pp. 1889–1894, Chengdu, 2016.

[14] Q. Qu, S. Wei, S. Liu, J. Liang, and J. Shi, "JRNet: jamming recognition networks for radar compound suppression jamming signals," *IEEE Transactions on Vehicular Technology*, vol. 69, no. 12, pp. 15035–15045, 2020.

[15] P. Wang, Y. Cheng, B. Dong, and G. Gui, "Binary neural networks for wireless interference identification," *IEEE Wireless Communications Letters*, vol. 11, no. 1, pp. 23–27, 2022.

[16] H. Xu, X. Ma, C. Wang et al., "A neural network approach for wireless spectrum anomaly detection in 5G-unlicensed network," *CCF Transactions on Pervasive Computing and Interaction*, pp. 1–9, 2022.

[17] T. J. O'Shea, T. Roy, and T. Erpek, "Spectral detection and localization of radio events with learned convolutional neural features," in *2017 25th European Signal Processing Conference (EUSIPCO)*, pp. 331–335, Kos, Greece, 2017.

[18] S. Rajendran, W. Meert, V. Lenders, and S. Pollin, "Unsupervised wireless spectrum anomaly detection with interpretable features," *IEEE Transactions on Cognitive Communications and Networking*, vol. 5, no. 3, pp. 637–647, 2019.

[19] R. Longadge and S. Dongre, "Class imbalance problem in data mining review," *International Journal of Computer Science & Network*, vol. 2, no. 1, 2013.

[20] B. Min, J. Yoo, S. Kim, D. Shin, and D. Shin, "Network anomaly detection using memory-augmented deep autoencoder," *IEEE Access*, vol. 9, pp. 104695–104706, 2021.

[21] G. Bovenzi, G. Aceto, D. Ciuonzo, V. Persico, and A. Pescapé, "A hierarchical hybrid intrusion detection approach in IoT scenarios," in *GLOBECOM 2020 - 2020 IEEE Global Communications Conference*, pp. 1–7, Taipei, Taiwan, December 2020.

[22] Y. Mirsky, T. Doitshman, Y. Elovici, and A. Shabtai, "Kitsune: an ensemble of autoencoders for online network intrusion detection," 2018, http://arxiv.org/abs/1802.09089.

[23] Q. Feng, Y. Zhang, C. Li, Z. Dou, and J. Wang, "Anomaly detection of spectrum in wireless communication via deep auto-encoders," vol. 73, Tech. Rep. 7, Journal of Supercomputing, 2017.

[24] Y. Ghanney and W. Ajib, "Radio frequency interference detection using deep learning," in *2020 IEEE 91st Vehicular Technology Conference (VTC2020-Spring)*, pp. 1–5, Antwerp, Belgium, May 2020.

[25] Y. Tian, H. Liao, J. Xu, Y. Wang, S. Yuan, and N. Liu, "Unsupervised spectrum anomaly detection method for unauthorized bands," *Space: Science & Technology*, vol. 2022, article 9865016, pp. 1–10, 2022.

[26] C. Huang, Z. Yang, J. Wen et al., "Self-supervision-augmented deep autoencoder for unsupervised visual anomaly detection," *IEEE Transactions on Cybernetics*, pp. 1–14, 2021.

[27] B. Zong, Q. Song, M. R. Min et al., "Deep autoencoding Gaussian mixture model for unsupervised anomaly detection," in *International Conference on Learning Representations*, Vancouver, Canada, 2018.

[28] F. Ye, C. Huang, J. Cao, M. Li, Y. Zhang, and C. Lu, "Attribute restoration framework for anomaly detection," *IEEE Transactions on Multimedia*, vol. 24, pp. 116–127, 2022.

[29] D. Gong, L. Liu, V. Le et al., "Memorizing normality to detect anomaly: memory-augmented deep autoencoder for unsupervised anomaly detection," in *2019 IEEE/CVF International Conference on Computer Vision (ICCV)*, pp. 1705–1714, South Korea, 2019.

[30] L. Zhang, H. Wang, and T. Li, "Anti-jamming message-driven frequency hopping—part I: system design," *IEEE Transactions on Wireless Communications*, vol. 12, no. 1, pp. 70–79, 2013.

[31] Z. Chen and L. Wu, "Blind source separation of dual-carrier MPPSK signal based on smoothed pseudo wigner distribution," in *2014 9th International Symposium on Communication Systems, Networks Digital Sign (CSNDSP)*, pp. 664–667, Manchester, UK, July 2014.

[32] V. Bajaj, K. Rai, A. Kumar, and D. Sharma, "Time-frequency image based features for classification of epileptic seizures from EEG signals," *Biomedical Physics & Engineering Express*, vol. 3, no. 1, p. 015012, 2017.

[33] Y. Zhou, X. Song, Y. Zhang, F. Liu, C. Zhu, and L. Liu, "Feature encoding with autoencoders for weakly supervised anomaly detection," *IEEE Transactions on Neural Networks and Learning Systems*, vol. 33, no. 6, pp. 1–12, 2021.

[34] F. Wan, G. Guo, C. Zhang, Q. Guo, and J. Liu, "Outlier detection for monitoring data using stacked autoencoder," *IEEE Access*, vol. 7, pp. 173827–173837, 2019.

[35] T. Kuang, H. Chen, L. Han, R. He, W. Wang, and G. Ding, "Abnormal signal recognition with time-frequency spectrogram: a deep learning approach," 2022, http://arxiv.org/abs/2205.15001.

[36] M. Liu, Z. Liu, W. Lu, Y. Chen, X. Gao, and N. Zhao, "Distributed few-shot learning for intelligent recognition of communication jamming," *IEEE Journal of Selected Topics in Signal Processing*, vol. 16, no. 3, pp. 395–405, 2022.

[37] T. M. Barros, P. A. Souza Neto, I. Silva, and L. A. Guedes, "Predictive models for imbalanced data: a school dropout perspective," *Education Sciences*, vol. 9, no. 4, p. 275, 2019.